Resource

Chemistry & Biology

A 45-Amino-Acid Scaffold Mined from the PDB for High-Affinity Ligand Engineering

Graphical Abstract

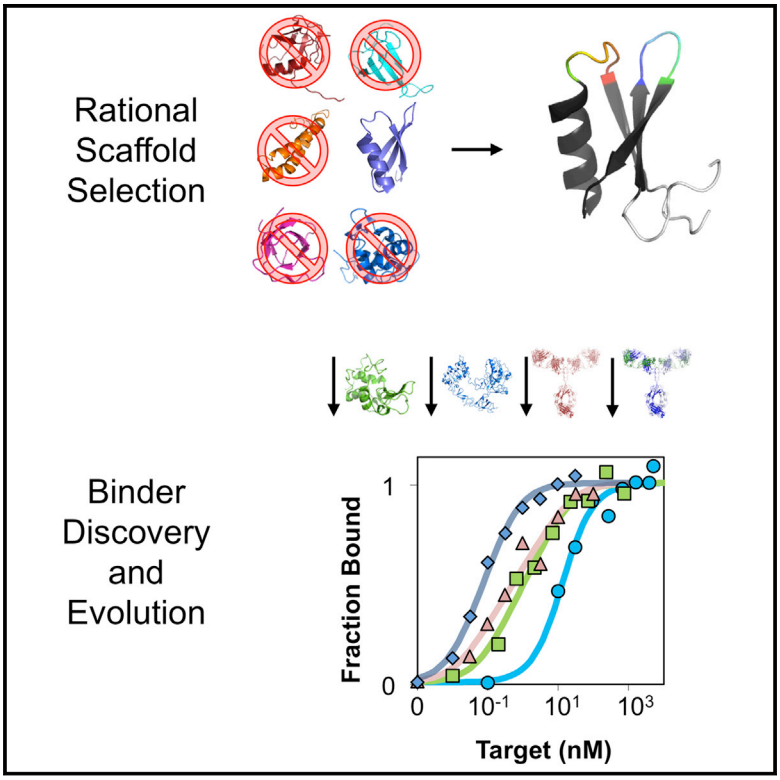

Authors

Max A. Kruziki, Sumit Bhatnagar, Daniel R. Woldring, Vandon T. Duong, Benjamin J. Hackel

Correspondence

hackel@umn.edu

In Brief

Kruziki et al. present a small protein scaffold (Gp2) that enables simple de novo ligand discovery and evolution toward multiple targets. Gp2 uniquely combines robust evolution, small size (45 amino acids), nanomolar affinity, and high thermal stability.

Highlights

- Systematic search of PDB for small, evolvable protein as a binding scaffold
- Gp2 with 45 amino acids has small size, ease of evolution, and stability
- De novo discovery of high-affinity, specific Gp2 binders toward four targets
- Gp2 evolved to target epidermal growth factor receptor

Kruziki et al., 2015, Chemistry & Biology 22, 946–956
July 23, 2015
http://dx.doi.org/10.1016/j.chembiol.2015.06.012

CellPress

CellPress

Chemistry & Biology
Resource

A 45-Amino-Acid Scaffold Mined from the PDB for High-Affinity Ligand Engineering

Max A. Kruziki,[1] Sumit Bhatnagar,[1] Daniel R. Woldring,[1] Vandon T. Duong,[1] and Benjamin J. Hackel[1,*]
[1]Department of Chemical Engineering and Materials Science, University of Minnesota, Minneapolis, MN 55455, USA
*Correspondence: hackel@umn.edu
http://dx.doi.org/10.1016/j.chembiol.2015.06.012

SUMMARY

Small protein ligands can provide superior physiological distribution compared with antibodies, and improved stability, production, and specific conjugation. Systematic evaluation of the PDB identified a scaffold to push the limits of small size and robust evolution of stable, high-affinity ligands: 45-residue T7 phage gene 2 protein (Gp2) contains an α helix opposite a β sheet with two adjacent loops amenable to mutation. De novo ligand discovery from 10^8 mutants and directed evolution toward four targets yielded target-specific binders with affinities as strong as 200 ± 100 pM, T_ms from 65°C ± 3°C to 80°C ± 1°C, and retained activity after thermal denaturation. For cancer targeting, a Gp2 domain for epidermal growth factor receptor was evolved with 18 ± 8 nM affinity, receptor-specific binding, and high thermal stability with refolding. The efficiency of evolving new binding function and the size, affinity, specificity, and stability of evolved domains render Gp2 a uniquely effective ligand scaffold.

INTRODUCTION

Molecules that bind targets specifically and with high affinity are useful clinically for imaging, therapeutics, and diagnostics as well as scientifically as reagents for biological modulation, detection, and purification. Antibodies have been successfully used for these applications in many cases, but their drawbacks have instigated a search for alternative protein scaffolds from which improved binding molecules can be developed (Banta et al., 2013; Stern et al., 2013). Biodistribution mechanisms such as extravasation (Schmidt and Wittrup, 2009; Yuan et al., 1995) and tissue penetration (Thurber et al., 2008a, 2008b) are limited by large size (150 kDa for immunoglobulin G, 50 kDa for antigen-binding fragments, and even 27 kDa for single-chain variable fragments), thereby reducing delivery to numerous locales including many solid tumors. In addition, large size and FcRn-mediated recycling slow plasma clearance (Lobo et al., 2004). While beneficial for minimally toxic molecular therapeutic applications, slow clearance greatly hinders molecular imaging and systemically toxic therapeutics such as radioimmunotherapy (Wu and Senter, 2005) via high background. Smaller agents yield improved results (Natarajan et al., 2013; Orlova et al., 2009; Zahnd et al., 2010). Moreover, small size does not preclude therapeutic applications where blocking a protein or protein interaction is required (Fleetwood et al., 2014). As scientific reagents, small size aids synthesis and selective conjugation, including protein fusion. Yet significant reduction in scaffold size increases the challenge of balancing evolved intermolecular interaction demands for affinity (Chen et al., 2013; Engh and Bossemeyer, 2002) or function while retaining beneficial intramolecular interactions for stability and solubility.

Protein scaffolds, frameworks upon which numerous functionalities can be independently engineered, offer a consistent source of binding reagents for the multitude of biomarkers and applications thereof (Banta et al., 2013; Sidhu, 2012; Stern et al., 2013). A successful protein scaffold should be efficiently evolvable to contain all of the following properties. High affinity (low-nanomolar dissociation constant) and specificity provide potent delivery (Schmidt and Wittrup, 2009; Zahnd et al., 2010), reduce side effects in clinical applications, and are requisite for precise use in biological study. Stable protein scaffolds provide tolerance to mutations in the search for diverse and improved function (Bloom et al., 2006), resistance to chemical and thermal degradation in production and synthetic manipulation, in vivo integrity to avoid immunogenicity and off-target effects (Hermeling et al., 2004; Rosenberg, 2006), and robustness to harsh washing conditions in vitro. Contrary to the multi-domain architecture of many antibodies and fragments, single-domain architecture facilitates production of native ligands as well as incorporation into protein fusions and other multicomponent systems. Cysteine-free structure allows for bacterial production in the reducing *Escherichia coli* cellular environment, intracellular stability in mammals, and the option of a genetically introduced thiol for site-specific chemical conjugation.

A multitude of alternative protein scaffolds have arisen that possess many of these beneficial properties (Table S1). Fibronectins (11 kDa) (Koide et al., 1998; Lipovsek, 2011), nanobodies (11 kDa) (Revets et al., 2005), designed ankyrin repeat proteins (20 kDa) (Tamaskovic et al., 2012), and anticalins (20 kDa) (Gebauer and Skerra, 2012) have been evolved to interact with numerous targets with high affinity while maintaining stability. However, the relatively large size of these scaffolds leaves room for potential improvement in solid tumor penetration and biodistribution through decreased size. Very small size has been achieved in the case of the cystine knottin scaffold (20–50 amino acids) (Moore et al., 2012) and cyclic peptides (17 amino acids) (Heinis et al., 2009). Knottins often use grafting of known binding motifs, which is only applicable to a subset of targets (Ackerman et al., 2014), although binders have been

evolved from naive libraries (Getz et al., 2011). Peptides, partially due to limited potential for interfacial area as well as the entropic cost of conformational flexibility (Castel et al., 2011), often require extensive optimization to yield the affinity and specificity required for many applications. In addition, the multiple disulfide bonds required for stabilization can complicate production and range of application in both cases. Slightly larger scaffolds, such as Fynomers (63 amino acids) (Grabulovski et al., 2007), affitin (65 amino acids) (Mouratou et al., 2007), or sso7d (63 amino acids) (Gera et al., 2011), have moved closer to the small size of knottins and bicyclic peptides without the need for disulfides. Affibodies (58 amino acids) are the smallest heavily investigated disulfide-free scaffold in the literature (Löfblom et al., 2010). Their helical paratope has provided high affinity toward many targets; however, they are typically severely destabilized after mutation (midpoint of thermal denaturation [T_m] range, 37°C–65°C; median, 46°C) (Hackel, 2014). There is still space to develop a scaffold that approaches the small size of knottins and peptides but also possesses the other beneficial properties.

We hypothesized that a thorough exploration of known protein topologies could reveal an effective scaffold that pushed current limits of small size with potential for high affinity and retention of stability. A search of the PDB was performed to identify a small protein with characteristics amenable to use as a protein scaffold, including retention of stability upon mutation, lack of disulfides, and large available binding surface. Gene 2 protein from T7 phage was selected as the scaffold to investigate further, based on the considered characteristics. A library of truncated gene 2 protein (Gp2) mutants was created by diversifying two solvent-exposed loops in the protein. Using yeast surface display and affinity maturation, target-specific Gp2 molecules with nanomolar or better affinity to three model proteins were isolated. The binding proteins retained the wild-type secondary structure characteristics and remained folded up to an average 72°C. These results verified Gp2 as a promising scaffold for the isolation of strong, specific binders to a wide variety of targets and motivated ligand discovery for the cancer biomarker epidermal growth factor receptor (EGFR). EGFR is a clinical biomarker for imaging and therapy due to its overexpression in multiple cancer types, including head and neck, breast, bladder, prostate, kidney, colorectal, non-small cell lung cancer, and glioma carcinoma (Corcoran and Hanson, 2013; Hynes and MacDonald, 2009). Improved EGFR targeting could empower molecular imaging for patient stratification (Laurent-Puig et al., 2009; Moroni et al., 2005; Scartozzi et al., 2009) and treatment monitoring as well as advanced therapeutics. An EGFR-binding Gp2 was isolated and matured. Binding was verified for membrane-bound EGFR on mammalian cells, and Gp2 was used to detect relative EGFR expression levels across multiple cell lines. The unique combination of small size and efficient evolution of high affinity and stability give Gp2 significant potential for the development of molecular targeting agents.

RESULTS

Scaffold Discovery and Library Construction

The structural information in the PDB was surveyed to locate potential binding scaffolds. Based on the efficacy of diversifying loops at one end of a β sandwich in antibody domains and the type III fibronectin domain, we sought scaffolds with solvent-exposed loops on a β-sheet-rich framework. As two loops can provide sufficient diversity for high-affinity binding while a single loop is often insufficient (Lipovsek et al., 2007), we sought protein topologies with two adjacent loops amenable to mutation. All proteins in the PDB were filtered to identify single domains of 40–65 amino acids and at least 30% β-sheet content, although the PDB filter also anomalously returned several proteins as large as 70 amino acids and with only 25% β-sheet content. Resultant proteins were visualized in PyMol. Those with two adjoining loops (regions of at least four amino acids without defined secondary structure) and no disulfide bonds were retained. The potential of the diversified loops to provide sufficient binding interface while maintaining a folded protein was assessed via two metrics: (1) solvent-accessible surface area of the loop amino acids was calculated using serine as the side-chain basis for all diversified sites to avoid wild-type sequence bias; and (2) the average destabilization upon random mutation of the loops was computed using Eris (Yin et al., 2007). Multiple proteins exhibited favorable properties within several categories (Figure 1). One scaffold that performed well on all criteria, especially differentiated by loop orientation, surface area (709 Å^2, second highest), and stability ($\Delta\Delta G_{f,mut}$ = 5.6 kcal/mol, third lowest), was selected for focused investigation: T7 phage gene 2 protein (Cámara et al., 2010).

T7 phage gene 2 protein, an *E. coli* RNA polymerase inhibitor from T7 phage with 64 amino acids, was the top protein selected by the ranking system (Figure 2). The coils at the N and C termini (14 and 5 amino acids, respectively) were genetically removed to minimize protein size. In addition, a framework mutation (I17V) was made on the basis of 59% frequency in naturally occurring homologs and computational stabilization ($\Delta\Delta G_{f,I\rightarrow V}$ = −3.8 kcal/mol via Eris; Yin et al., 2007). These modifications resulted in the 5.2-kDa, 45-amino-acid Gp2 scaffold.

To evaluate the potential of Gp2 as a protein scaffold for molecular recognition, a combinatorial library of selectively randomized Gp2 sequences was constructed for use in discovery and directed evolution. Two loops, comprising amino acids E7-S12 and V34-E39 (Figure 2), were selected as the proposed binding surface, based on their lack of defined secondary structure, continuous solvent-exposed face, and high solvent-exposed surface area (709 Å^2). A yeast surface displayed library, containing approximately 4 × 10^8 Gp2 molecules based on the number of yeast transformants, was constructed by randomizing six amino acids from each loop using amino acid frequencies consistent with antibody complementarity-determining regions (CDRs) (Hackel et al., 2010), and allowing loop length diversity of six, seven, or eight amino acids in each loop (Figure 2). Hemagglutinin (HA) and c-MYC epitope tags placed upstream and downstream of the Gp2 gene, respectively, allowed for differentiation through flow cytometry of yeast that lost the plasmid (HA$^-$/c-MYC$^-$), yeast carrying a plasmid with incomplete Gp2 (HA$^+$/c-MYC$^-$), and yeast expressing full-length Gp2 (HA$^+$/c-MYC$^+$). A quality control check by flow cytometry indicated that 44% of yeast harboring plasmid expressed full-length Gp2. This was supported through sequencing Gp2 genes, resulting in four full-length Gp2 genes, one Gp2 containing stop codon in the diversified loop and five frameshifted genes. Therefore, the actual size of the library was 1.8 × 10^8 unique, full-length Gp2

A

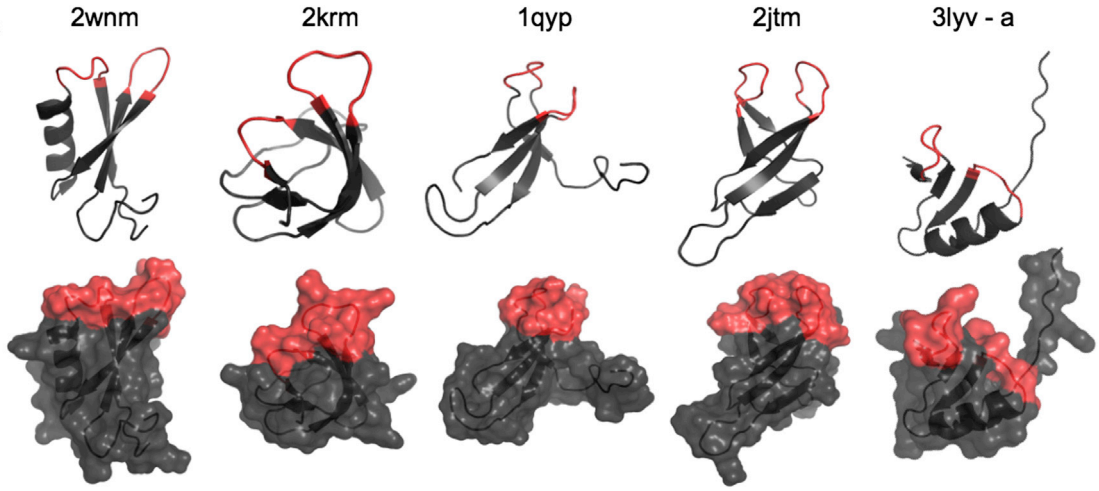

B

PDB ID	Amino Acids	% β strand	% α Helix	Loop 1	Loop 2	Loop 1 Length	Loop 2 Length	Loop ASA (Å^2)	ASA / Residue (Å^2)	$\Delta\Delta G_{f,mut}$ (kcal/mol)
2wnm	64	32	21	41 - 46	68 -73	6	6	709	11.1	5.6
2krm	57	45	5	31 - 37	50 - 54	7	5	605	10.6	1.9
1qyp	57	33	0	19 -23	47 - 51	5	5	609	10.7	3.3
2jtm	60	43	0	11 - 17	43 - 49	7	7	676	11.3	7.7
3lyv - a	66	30	13	26 - 30	47 - 51	5	5	724	11.0	7.3
2kr3	70	45	4	36 - 41	62 - 66	6	5	582	8.3	8.0
2rqt	61	54	4	1099 - 1104	1120 - 1124	6	5	444	7.3	8.3
2rpn	59	42	5	6 - 10	20 - 25	5	6	359	6.1	7.9
3kz5 - b	52	34	28	281 - 284	298 - 303	4	6	318	6.1	7.8
1zrp	53	28	16	5 - 10	38 - 43	6	6	416	7.8	9.7
3i9q	57	49	5	35 - 41	54 - 58	7	5	564	9.9	9.9
3kyu	54	25	16	5 - 10	38 - 43	6	6	339	6.3	10
3m0p	62	45	4	35 - 41	54 - 58	7	5	534	8.6	9.9
3ngp	62	45	4	36 - 41	54 - 58	6	5	598	9.6	10
1ttg	94	45	0	[a]	[a]	[a]	[a]	1640	17.4	8.5
2b88	58	0	67	[b]	[b]	[b]	[b]	800	13.8	4.4

[a] Fibronectin has a three loop proposed paratope (23-31, 52-56, and 76-86).
[b] Affibody has a helix surface proposed paratope (9-11, 13, 14, 17, 18, 24, 25, 27, 28, 32, and 35)

Figure 1. Summary of Information for Top Potential Scaffolds

(A) Structure and proposed paratope surface (red) of top five scoring scaffolds. Images created in PyMol.

(B) PDB ID, amino acid length, % β strand, and % α helix are all from the PDB. Loop residues are identified as residues between secondary structural elements. Loop accessible surface area (ASA) is calculated using GetArea after mutating loop residues to serines within PyMol. $\Delta\Delta G_{f,mut}$ was calculated for random loop mutants using Eris. Fibronectin (1ttg) and Affibody (2b88) are included for comparison. See also Table S1 for commonly used scaffolds.

proteins. Amino acid diversity matched the designed distribution (median absolute deviation, 0.5%; Figure S1).

Yeast Surface Display Selection against Model Protein Targets

Lysozyme and immunoglobulin G (IgG) from rabbit and goat were chosen as the first targets for evaluating the binding potential of the Gp2 scaffold. The differing size and surface topologies of lysozyme (14 kDa) and the IgG proteins (150 kDa) test the ability of the scaffold to target diverse proteins (Diamond, 1974; Harris et al., 1998). The similarity of the two IgG proteins test the ability of Gp2 to create very specific ligands, i.e. binding to goat IgG but not rabbit IgG and vice versa.

During each evolutionary round, the Gp2 library underwent two sorts to enrich specific binders (either with target-coated magnetic beads or through fluorescence-activated cell sorting [FACS]) and one c-MYC$^+$ sort to isolate full-length Gp2. Sorted Gp2 sequences were mutated through parallel error-prone PCR reactions targeting the loops or the entire gene and transformed into yeast with loop shuffling driven by homologous

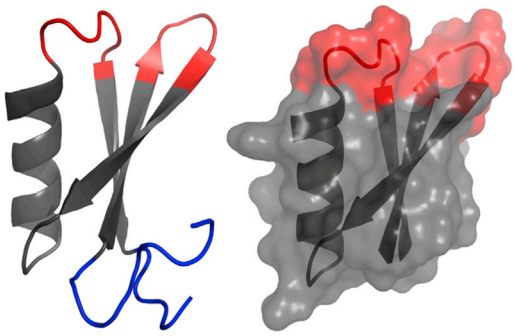

Wild-type:
MSNVNTGSLSVDNKKFWATVESSEHSFEVPIYAE
TLDEALELAEWQYVPAGFEVTRVRPCVAPK

Library:
KFWATVX_{6-8}FEVP**V**YAETLDEALE
LAEWQYX_{6-8}VTRVRP

Figure 2. Solution Structure of Gp2

Diversified amino acids are highlighted in red and underlined in sequence. The N- and C-terminal tails removed to create the Gp2 scaffold are highlighted in blue. An I17V (boldface in sequence) mutation was added based on prevalence in homologous protein sequences. Images created in Macpymol (PDB: 2WNM).

recombination (Hackel et al., 2010). After a single maturation cycle, clear binding was evident by flow cytometry for each target campaign (data not shown). Two to four rounds of selection and mutation were carried out for each target to isolate binders with low-nanomolar to picomolar affinity.

Single clones were isolated at the end of rounds where strong binding was detectable by FACS. Target affinity on the surface of yeast was determined by concentration titration (Table 1; Figure 3A). Affinities measured on the surface of yeast have been previously shown to match affinities measured by surface plasmon resonance and related techniques (Gai and Wittrup, 2007). The goat IgG-binding population contained one dominant sequence family that had affinities as strong as 200 ± 100 pM after one mutagenic cycle. The rabbit IgG-binding population contained a family of low-nanomolar affinity binders at the end of the third mutagenic cycle, which improved to 2.3 ± 1.4 nM after another round of affinity maturation. A single dominant clone group was isolated for lysozyme binders after the second round of mutagenesis, albeit with weaker binding. Lysozyme-binding clones isolated in subsequent rounds showed point mutations but no significant increase in binding affinity. A sublibrary was created in which amino acid diversity was chosen based on weighted scores of parental binding sequences, computational stability analysis (using FoldX), natural homolog sequences, and potential for complementarity (Figure S2). The strongest library member isolated was GαLys$_{A0.3.3}$ with an affinity of 0.9 ± 0.7 nM (Figure 3A). During selection and maturation, the lysozyme target was always displayed as a complex with streptavidin. Resultantly, GαLys$_{A0.3.3}$ bound to a streptavidin-lysozyme complex but not streptavidin or lysozyme alone. Nevertheless, this still supports Gp2 as able to generate specific, high-affinity binders to the target presented.

To examine target specificity, the strongest binding ligand from each target campaign was incubated with four proteins at 1 μM. All Gp2 proteins show strong binding to the target protein for which they were selected and matured, while showing fluorescence only slightly above background signal for the three other proteins (Figure 3B). Four depletion sorts were performed per round, consisting of two sorts to bare streptavidin-coated beads and two sorts to non-target protein-coated beads. This sorting process enabled only Gp2 binders to the protein of interest to be carried through the affinity maturation process.

Soluble Protein Characterization

To examine whether untethered Gp2 will retain its useful properties, the protein was produced and tested for binding and stability. Wild-type Gp2 could not be produced at detectable levels in a typical production *E. coli* strain, likely due to the native RNA polymerase inhibition function of the protein (Nechaev and Severinov, 1999). However, mutated clones were able to be produced, presumably due to mutation of many of the residues on Gp2 normally required to interact with DNA during transcription inhibition (Cámara et al., 2010). Protein titer, with no optimization, varied between 0.2 and 2.2 mg/l for different Gp2 mutants. The JE1 *E. coli* strain has the β-jaw portion of the *E. coli* RNA polymerase protein deleted (Ederth et al., 2002), and enabled production of wild-type Gp2 at 0.7 mg/l. All Gp2 molecules were verified by mass spectrometry to within 0.1% of the expected mass.

Structure and stability after mutation are important qualities of a potential protein scaffold. To evaluate secondary structure changes after Gp2 was evolved for new binding function, circular dichroism measurements were taken of the top binder for each target. The ellipticity spectra of the binding Gp2 proteins deviate only slightly from those of wild-type Gp2, suggesting that the secondary structure remains relatively unchanged after multiple mutations in the backbone and entirely new loop regions

Table 1. Characterization of Wild-Type Gp2 and the Top Binding Molecule for Each Target

Name	Loop 1	Loop 2	Framework	$K_{D,yeast}$ (nM)	$K_{D,soluble}$ (nM)	T_m (°C)
Wild-type	ESSEHS	VPAGFE	–	–	–	67 ± 1
GαGIgG$_{2.2.1}$	YDYDADYY	YSNHSDYL	E30V, Q32R	0.2 ± 0.1	0.4 ± 0.3	70 ± 4
GαLys$_{A0.3.3}$	FSYGNL	SGAYEY	–	0.9 ± 0.7	ND	65 ± 3
GαRIgG$_{3.2.3}$	HSVHGY	GNALGY	E30F, W31G	2.3 ± 1.4	1.0 ± 0.5	80 ± 1

Loop 1 and Loop 2 indicate amino acid sequences in the diversified loops (E7-S12 and V34-E39). Framework indicates mutations outside of the loops resulting from error-prone PCR during evolution. K_D values represent equilibrium dissociation constants for clones displayed on the surface of yeast or as purified soluble protein (±SD for n ≥ 3). T_m indicates the midpoint of thermal denaturation as measured by circular dichroism (±SD for n = 2). ND, data not determined.

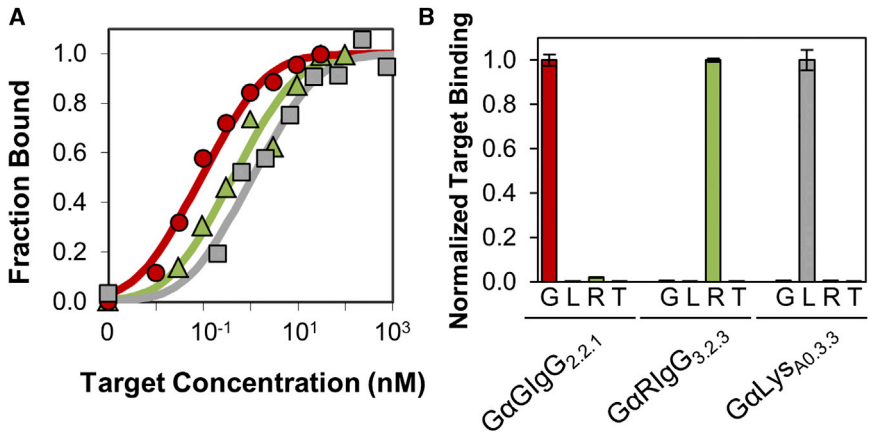

Figure 3. Binding Characterization

(A) Yeast displaying GαGIgG$_{2.2.1}$ (red circles), GαRIgG$_{3.2.3}$ (green triangles), and GαLys$_{A0.3.3}$ (gray squares) were incubated with the indicated concentrations of biotinylated target. Binding was detected by streptavidin-fluorophore via flow cytometry. Titration indicates equilibrium dissociation constants of 0.2 ± 0.1, 2.3 ± 1.4, and 0.9 ± 0.7 nM.

(B) Yeasts were incubated with 1 μM goat IgG (G), lysozyme (L), rabbit IgG (R), or transferrin (T). Binding was detected by streptavidin-fluorophore via flow cytometry. Data are normalized to signal of intended target for each yeast strain. Error bars represent ±SD of n = 3 samples. See Figure S3 for full collection of affinity titration curves.

(Figure 4A). The midpoint of thermal denaturation of each protein was measured by monitoring the loss of secondary structure at 218 nm as temperature increased (Table 1; Figure 4B). Interestingly, the average stability of Gp2 binding mutants increased by 5°C over wild-type Gp2, which had a T_m = 67°C ± 1°C. Gp2 mutants raised to 98°C and brought down to room temperature had circular dichroism spectra similar to the initial measurements (Figure 4A). GαGIgG$_{2.2.1}$ (containing a framework mutation, R44E, to increase production) maintained binding activity (Figure 4D) after reverse-phase high-performance liquid chromatography (HPLC) and heating to 98°C, illustrating the chemical and thermal stability of the protein.

The binding affinities of select soluble Gp2 clones, measured by equilibrium competition titration, were 0.4 ± 0.3 nM for GαGIgG$_{2.2.1}$ and 1.0 ± 0.5 nM for GαRIgG$_{3.2.3}$ (Table 1; Figure 4C), showing good agreement with the K_Ds obtained from yeast surface display affinity titration.

EGFR-Targeting Gp2 Domains

The success and ease of ligand discovery for the three model targets from the current Gp2 library motivated the search for a Gp2 ligand that strongly and specifically bound EGFR for use in cancer imaging or treatment. Through methods similar to model targeting, Gp2 ligand discovery was performed using soluble biotinylated EGFR ectodomain as the target. After the second round of affinity maturation, strong binding was evident by flow cytometry with 50 nM soluble EGFR (Figure 5A). Deep sequencing indicated that GαEGFR$_{2.2.3}$ was the dominant clone in the library, and revealed several other families of sequences that were enriched during evolution. Purified Gp2-EGFR$_{2.2.3}$ binds to intact membrane-bound EGFR with an affinity of 18 ± 8 nM as measured by labeling A431 epidermoid carcinoma cells (Figure 5B) that highly overexpress EGFR on their surface (Hackel et al., 2012; Spangler et al., 2010). Gp2-EGFR$_{2.2.3}$ exhibits secondary structure consistent with the wild-type Gp2 domain (Figure 4C) and is thermally stable (T_m = 71°C ± 2°C, Figure 5C). Fluorescence microscopy was used to evaluate binding specificity. GαEGFR$_{2.2.3}$, but not wild-type Gp2, effectively labels the cell surface of EGFR^{high} A431 epidermoid carcinoma cells but not EGFR^{low} MCF7 mammary carcinoma cells (Figure 5D). Moreover, binding of biotinylated GαEGFR$_{2.2.3}$ was blockable by excess unlabeled Gp2 (Figure 5E). Gp2 biotinylation was straightforward (with *N*-hydroxy succinimide biotin) due to the lone lysine residue at the N terminus. To further validate that the evolved Gp2 domain can differentiate between different EGFR levels, four cell lines, A431 epidermoid carcinoma (EGFR^{high}), MDA-MB-231 mammary carcinoma (EGFR^{mid}), DU145 prostate carcinoma (EGFR^{mid}), and MCF7 mammary carcinoma (EGFR^{low}), were labeled with GαEGFR$_{2.2.3}$ and a secondary fluorophore. Fluorescence signal correlated with the cell surface expression level of EGFR (Figure 5F).

Deep Sequencing of Naive and Binding Populations

Deep sequencing was performed on the original library and the first enriched population in each target campaign that displayed significant selective binding represented by a 10:1 ratio of cells on target beads to control beads. Multiple binding sequence families were identified for each target (4,209 unique sequences in 153 families identified by 85% sequence identity). Site-wise changes in amino acid frequencies, relative to the original library, for heavily diversified loops (Figure 6A) and framework sites subject to error-prone PCR (Figure 6B) reveal site-specific amino acid preferences. In addition, loop length frequency shows a slight change from the initial library to the evolved binders (Figure 6C).

DISCUSSION

We sought to identify a protein scaffold with a unique combination of small size and robust evolvability of specific, high-affinity binding while retaining stability, and sought to evaluate the ability to identify such a scaffold via systematic analysis of protein topology and an estimation of mutational tolerance. Gp2 provides very small size (5 kDa, 45 amino acids) and has been efficiently evolved, to four different targets, to picomolar to nanomolar affinities with good specificity including strong discrimination between related IgGs. Evolved molecules exhibit good thermal and chemical stability (T_m = 65°C–80°C with reversible unfolding and tolerance to reverse-phase chromatography) and are functional in cellular assays. Gp2 succeeded with the combination of an effective topology, diversification design (tolerant loops of sufficient size, antibody-inspired amino acid bias, and shape diversity via loop length variation), and evolution method.

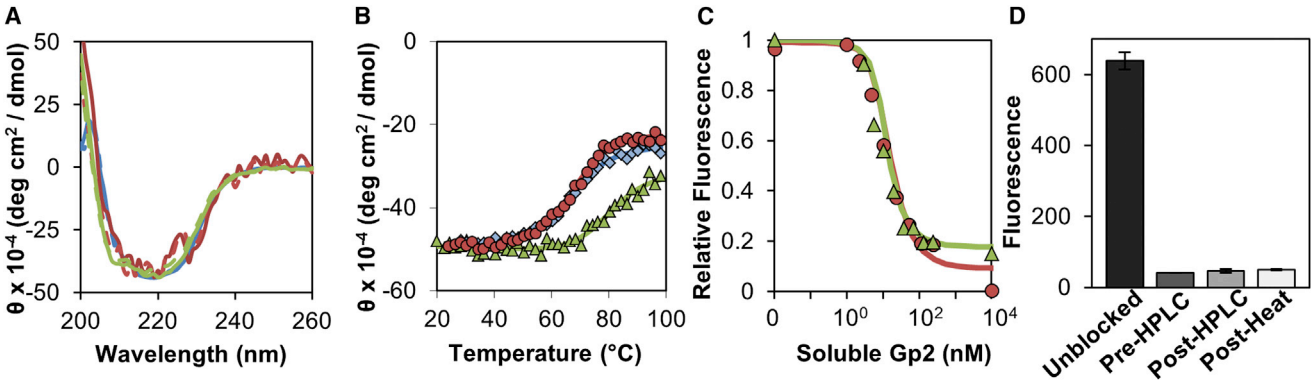

Figure 4. Soluble Gp2 Characterization

(A and B) Purified Gp2 clones (blue, wild-type; red, GαGIgG2.2.1; green, GαRIgG3.2.3) were analyzed by circular dichroism spectroscopy. (A) Molar ellipticity (θ) was measured at indicated wavelengths before (solid lines) and after (dashed lines) thermal denaturation. (B) Molar ellipticity was monitored at 218 nm upon heating from 25°C to 98°C at 1°C per minute.

(C) Biotinylated IgG (2 nM goat or 4 nM rabbit as appropriate) was incubated with the indicated concentration of purified Gp2 and used to label yeast displaying the corresponding Gp2 clone. IgG binding was measured by streptavidin-fluorophore via flow cytometry.

(D) Purified GαGIgG2.2.1 was subjected to various treatments prior to use in the competitive binding assay (as in C). Unblocked is a control without Gp2 competition. Pre-HPLC uses competition by GαGIgG2.2.1 that was purified on a metal affinity column. Post-HPLC uses competition by GαGIgG2.2.1 purified by metal affinity chromatography and reverse-phase high-performance liquid chromatography and lyophilization. Post-heat uses competition by GαGIgG2.2.1 purified as in Post-HPLC along with heating to 98°C and cooling back to 22°C. Error bars are ±SD on n = 2 samples. See Figure S2 for $G\alpha Lys_{A0.3.3}$.

The particular topology of an α helix opposite a three-strand β sheet underpinning two diversified loops is a new structure for a generalized binding scaffold. Of course, loops have been successful with numerous other topologies including—as examples rather than an all-inclusive list—antibodies, fibronectin domains, and GFP (Pavoor et al., 2009). Yet not all loop-presenting frameworks are equally efficacious, as evidenced by the varying performance of different scaffolds (Binz et al., 2005). Of note here, the second candidate in our theoretical scaffold evaluation, an SH3 domain from CD2 associated protein (Roldan et al., 2011), has substantially different framework topology and loop orientation (Figure 1). This SH3 domain is a homolog (root-mean-square deviation = 1.4 Å and TM score = 0.79, where >0.5 indicates similar fold; Zhang and Skolnick, 2005) of the Fynomer scaffold, which has been evolved for low-nanomolar affinity to five targets (Table S1) (Grabulovski et al., 2007; Panni et al., 2002). While the scaffold evaluation algorithm provides a framework for comparison, comparative experimental evaluation of numerous scaffolds is beyond the scope of the current study. Importantly, the demonstrated efficacy of Gp2 provides evidence of an improved ability to merge design goals in evolutionary capacity, affinity, and stability if the topology is properly selected.

Regarding evolutionary library design, while the diversified loops provided sufficient diversity for high-affinity binding, adjacent framework mutations in several clones were noted (Table 1). Deep sequencing suggests that added diversity at the N-terminal edge of the second loop could be beneficial, as E30, W31, and Q32 exhibited higher than average variance in binders relative to the naive library ($p < 0.001$), presumably resulting from error-prone PCR during evolution (Figure 6B). In addition, K1 also exhibits an increased mutation rate ($p = 0.006$), perhaps to account for change in exposure or structure due to the removal of the N-terminal tail. Conversely, lower than average mutation rates of sites F2, A4, P16, A25, Y33, and V40 ($p < 0.001$) suggest an evolutionary benefit to conservation at those sites. Notably, Y33 and V40 directly flank the diversified region of the second loop and are relatively buried in the protein core (19% and 21% solvent accessibility, respectively), suggesting a loop-anchoring benefit. Overall, mutation tolerance correlated with solvent accessibility ($p = 0.001$, Figure S1). Antibody-inspired amino acid distribution was effective as it was closely maintained in binding sequences (Figure 6A), although evolutionary efficiency would benefit from slightly increased glycine, especially at select sites: amino acids 9–11 in the middle of the first loop and 34–35 at the start of the second loop. Meanwhile, evolutionary preference was evident for hydrophilic residues at sites 10 and 36 and hydrophobic residues at sites 12, 37, and 38. Loop length diversity was effectively utilized in binding sequences with a slight trend toward a longer first loop (18% decrease of wild-type 6-amino-acid length and 33% increase of 8-amino-acid loop; $p < 0.001$) and a second loop of wild-type length (12% increase; $p < 0.001$) (Figure 6C). Collectively, the diversification design was effective yet represents an avenue for improvement. While the Gp2 scaffold was robust in efficiently identifying effective binding molecules for each of the four disparate targets, one possible limitation is the modest number of lead molecules for each target. As scaffold size is reduced, the need to simultaneously optimize inter- and intramolecular interactions is heightened, and the solution space is diminished. While all evolved clones exhibited appropriate secondary structure, good thermal stability, and effective binding, the frequency of mutational tolerance of the naive library could be different. In fact, evolved proteins were readily produced in *E. coli*, albeit at moderate yields, and eight randomly selected initial library mutants were unable to be recovered in detectable amounts (data not shown), suggesting lack of solubility or stability in some naive mutants. Refining the combinatorial library using site-wise optimization of diversity based on the aforementioned data could improve the breadth of solutions.

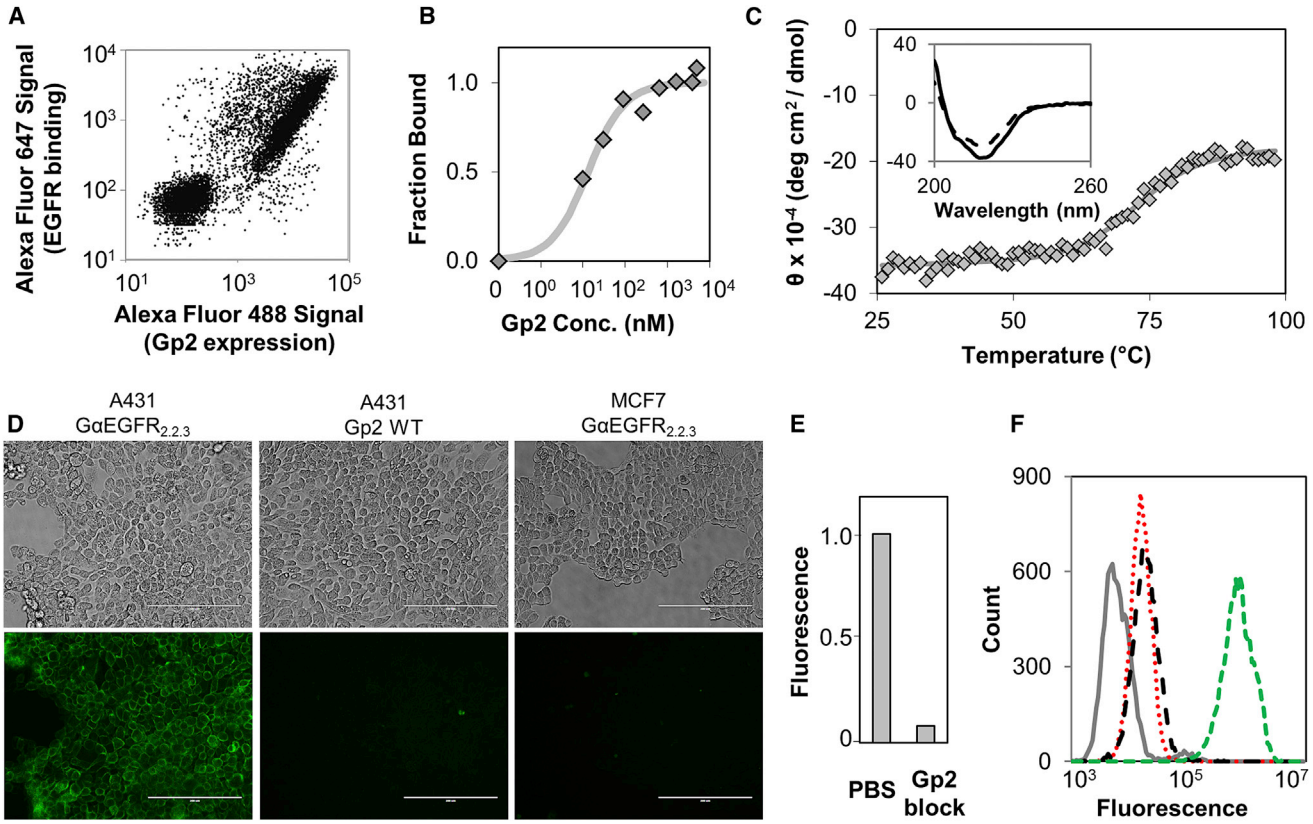

Figure 5. GαEGFR$_{2.2.3}$ Affinity and Stability

(A) Population of yeast displaying Gp2 incubated with 50 nM EGFR and anti-c-MYC antibody. Secondary fluorophores detect binding of EGFR and antibody. Spread of double-positive cells suggests moderate diversity of EGFR-binding Gp2 molecules. GαEGFR$_{2.2.3}$ was collected from top 1% of double positives.

(B) A431 cells were incubated with indicated amount of purified Gp2. Binding was detected by anti-His$_6$ fluorophore. Titration indicates an equilibrium dissociation constant of 18 ± 8 nM.

(C) Molar ellipticity was monitored at 218 nm upon heating from 25°C to 98°C at 1°C per minute. Molar ellipticity before (solid) and after (dashed) thermal denaturation is inset.

(D) Fluorescence microscopy of adhered cancer cell lines, incubated with 100 nM Gp2 protein and detected by anti-His$_6$-fluorescein. A431 cells labeled with GαEGFR$_{2.2.3}$ (left column) show localization to cell surface. A431 cells labeled with Gp2 WT (middle column) and MCF7 cells labeled with GαEGFR$_{2.2.3}$ (right column) show very little detectable binding. Scale bar represents 200 μm.

(E) A431 cells preincubated with PBS or 1 μM GαEGFR$_{2.2.3}$ and labeled with 200 nM biotinylated GαEGFR$_{2.2.3}$. Binding detected with streptavidin-fluorophore.

(F) Cancer cell lines expressing varying levels of EGFR: MCF7 with 2 × 10^4 receptors (gray line) (Reilly et al., 2000), MDA-MB-231 with 1 × 10^5 receptors (red dots) (Reilly et al., 2000), DU145 with 2 × 10^5 receptors (black dashes) (Malmberg et al., 2011), and A431with 3 × 10^6 (green dashes) (Spangler et al., 2010) were incubated with 1 μM GαEGFR$_{2.2.3}$ and detected with anti-His$_6$-fluorescein by flow cytometry.

Effective lead ligands, such as GαEGFR$_{2.2.3}$, which binds cellular EGFR with 18 ± 8 nM affinity and has high thermal stability (71°C), were identified. GαEGFR$_{2.2.3}$ was effective in cellular labeling for immunofluorescence, flow cytometry, and binding inhibition. Notably, GαEGFR$_{2.2.3}$ contains a single lysine at the N terminus, distal to the proposed binding paratope, for conjugation of imaging moieties or molecules of therapeutic interest. The conjugation of biotin to the molecule without strong inhibition of binding suggests that other molecules can similarly be conjugated. Similar small proteins have shown advantages over antibodies in molecular imaging of solid tumors (Natarajan et al., 2013; Orlova et al., 2009), for which enhanced transport and clearance afforded by small size are particularly valuable, and have exhibited clinical potential (Baum et al., 2010). It should be noted that, as with any synthetically engineered protein with non-human sequence components, immunogenicity of evolved molecules will need to be evaluated. Overall, Gp2 molecules represent a promising alternative with a unique blend of small size and robust evolution of stable, high-affinity binders.

SIGNIFICANCE

A systematic evaluation of the PDB based on size, protein secondary structure, paratope structure, and resilience to mutation led to further investigation of the small Gp2 domain. The ability to discover and evolve novel binding function on mutated Gp2 molecules is generalizable, with four targets currently tested. The small size, retention of thermal stability, and ease of evolving high-affinity binding provide a unique and powerful combination in an alternative scaffold. The Gp2 molecules reported here that bind strongly and specifically to rabbit IgG, goat IgG, lysozyme,

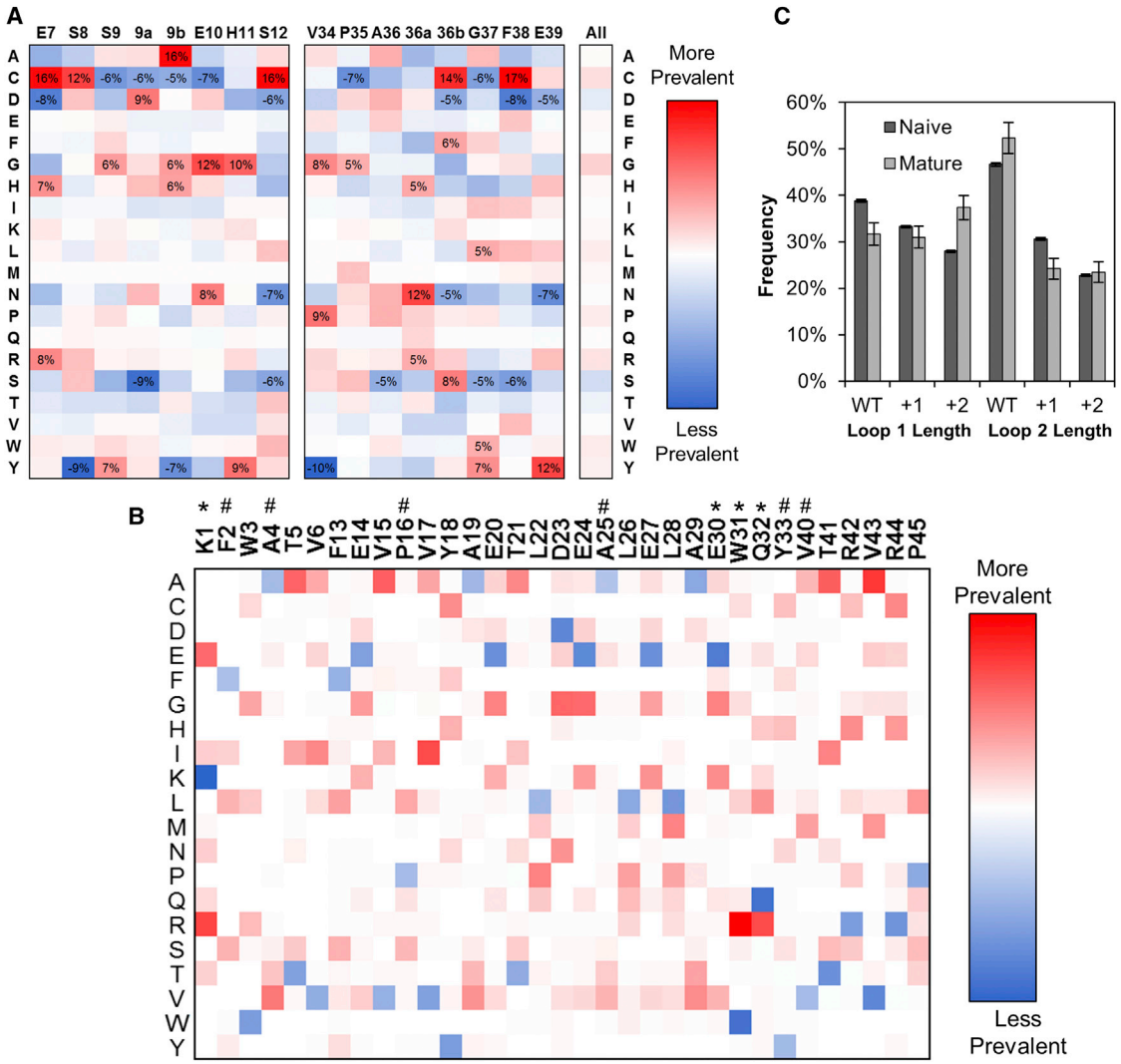

Figure 6. Deep Sequencing Comparison of Naive and Binding Populations

All sequences were grouped into families and damped.

(A) Diversified loop positions (CDR′) are shown at the top, with 9a and 9b, or 36a and 36b, representing loop length diversity positions. Positions with an absolute change of 5% or greater are labeled. All labeled positions have $p < 0.001$ ($n \geq 96$, number of damped sequences).

(B) Relative change in amino acid frequency by framework position from the naive library to combined mature populations. Certain mutations are more common than others due to error-prone PCR limitations. Positions where wild-type was conserved (#) or mutated (*) significantly more often ($p < 0.001$ for 3% deviation, $n \geq 421$) than the mean mutation rate are denoted.

(C) Frequency of Gp2 loop length in amino acids. The naive library was designed with equal loop length frequencies, but DNA bias during construction lead to overrepresentation of shorter loops. Mature combines high throughput sequencing from the four binding populations. All have $p < 0.001$. Error bars are ±SD for $n = 4.9 \times 10^4$ for naive and $n \geq 477$ for mature (number of damped sequences). See also Figure S1.

and EGFR have immediate use in biotechnology or, in the case of GαEGFR$_{2.2.3}$, as a potential clinical imaging agent, due to their single distal lysine available for conjugation of small molecules or other moieties. Moreover, deep sequencing of the binding populations provided insights on Gp2 evolution including mutational tolerance at non-loop positions and amino acid preference at individual loop positions. Overall, the initial successes of Gp2 combined with knowledge gained from sequence analysis suggest a promising scaffold that can be used to discover small, stable binders to many targets while providing an opportunity for ongoing study of evolutionary optimization of inter- and intramolecular interactions in a small scaffold.

EXPERIMENTAL PROCEDURES

Detailed experimental procedures are described in Supplemental Experimental Procedures.

PDB Analysis

All single domains within the PDB (accessed November 2011) were filtered to identify those with a size of 40–65 amino acids and at least 30% β sheet. Note that several proteins outside of these bounds were nevertheless returned by

the website's filter. PyMol (Schrödinger) was used to visualize the structures of the 259 remaining proteins, and those that contained two or more adjacent solvent-exposed loops whose surfaces formed one continuous face and had no disulfide bonds were further considered. The solvent-accessible surface area of the loop residues was calculated, using a 1.4-Å sphere, after mutating residues to serines in PyMol (Fraczkiewicz and Braun, 1998). For the top 14 proteins, the destabilization upon random mutation of the loop residues was calculated using Eris (Yin et al., 2007). Amino acid sequences were randomly generated using equal probability of each amino acid within the loops noted in Figure 1. Random mutants were analyzed until the mean destabilization converged within 0.25 kcal/mol for at least ten consecutive mutants (minimum 35 mutants in total). This resulted in a maximum of 84 mutants with a median of 42 mutants.

Library Construction

A genetic library was constructed based on a truncated form of T7 phage gene 2 protein, the top scoring protein, in which the sequence encoding for two loops was randomized using degenerate oligonucleotides encoding for an amino acid distribution mimicking antibody CDRs (Hackel et al., 2010). At diversified positions (Figure 1) the mixtures of nucleotides were 15% A and C, 25% G, and 45% T in the first position; 45% A, 15% C, 25% G, and 15% T in the second position; and 45% C, 10% G, and 45% T in the third position. The DNA was transformed into yeast surface display system strain EBY100 via homologous recombination with a pCT vector (Chao et al., 2006). The total number of transformants was determined through serial dilution on SD-CAA plates (0.07 M sodium citrate [pH 5.3], 6.7 g/l yeast nitrogen base, 5 g/l casamino acids, and 20 g/l glucose). Flow cytometry was used to determine the amount of full-length Gp2 displayed, through labeling of the N-terminal HA epitope and C-terminal c-MYC epitope, and supported with DNA sequence verification. The design of the focused lysozyme library is described in Supplemental Experimental Procedures.

Binder Selection and Affinity Maturation

Yeasts displaying the Gp2 library were exposed to control magnetic beads (first avidin-coated beads, then beads with immobilized non-target protein) to remove any non-specific binding interactions. Yeasts were then exposed to magnetic beads with immobilized biotinylated target protein (goat IgG, rabbit IgG, lysozyme, or EGFR ectodomain) and bound yeasts were selected. Magnetic sorts on the initial library were performed at 4°C and only one wash. Non-naive populations were sorted more stringently, at room temperature and with three washes. Flow cytometry selections, with biotinylated target protein and Alexa Fluor 647-conjugated streptavidin, were used (Hackel and Wittrup, 2010) to isolate full-length (c-MYC positive) Gp2 domain mutants that bind selectively and with high affinity toward the target proteins. Loop-focused and total gene error-prone PCR, using nucleotide analogs, and genetic loop shuffling between binding sequences were used to evolve improved function (Hackel et al., 2008).

Illumina MiSeq Analysis

Illumina MiSeq paired-end sequencing was conducted to obtain 4.9×10^4 reads from the naive library and a total of 6.4×10^5 (coefficient of variation = 24%) reads from binding populations. Loop 1 was analyzed independently from loop 2. Mature loop-1 sequences were grouped into 95 families (>60% sequence similarity) with 249 unique sequences, and after damping (quad rooted) the adjusted sequence count was $n \geq 173$ at each position. Mature loop-2 sequences were grouped into 96 families with 198 unique sequences, and after damping the adjusted sequence count was $n \geq 96$ at each position. Sequences from the naive library population were grouped into 4.9×10^4 families with 4.9×10^4 unique sequences, and after damping the adjusted sequence count was $\geq 1.1 \times 10^4$ (due to fewer sequences at extended loop positions). Mature framework analysis grouped the sequences into 153 families (>85% sequence similarity) with 4,209 unique sequences, and after damping the adjusted sequence count was $n \geq 421$ at each position. p values were calculated using a Welch t test while assuming a normal distribution and using the number of damped sequences at each position as the sample size.

Affinity and Biophysical Properties

Binding affinities of evolved Gp2 molecules were determined by titrating target and evaluating binding using yeast surface display and flow cytometry (Chao et al., 2006). For $G\alpha Lys_{A0.3.3}$ Alexa Fluor 488-conjugated streptavidin was mixed equimolarly with singly biotinylated lysozyme at 2 μM prior to titration and yeast labeling. Gp2 domains were produced in *E. coli*, using strain JE1(DE3) for wild-type or BL21(DE3) for other Gp2 domains, purified by metal affinity chromatography and reverse-phase HPLC, and verified by mass spectrometry. Purified Gp2 was suspended at 0.2–0.9 mg/ml in PBS (8.0 g/l NaCl, 0.2 g/l KCl, 1.44 g/l Na_2HPO_4, 0.24 g/l KH_2PO_4 [pH 7.2]) or 10 mM sodium acetate (pH 5.5), and secondary structure and thermal stability were evaluated by wavelength (200–260 nm) and temperature scans (25–98°C at 218 nm) via circular dichroism spectroscopy. Binding affinity was further measured by equilibrium competition titration with purified Gp2, target protein, and Gp2 displayed on the yeast surface using flow cytometry (Lipovsek et al., 2007). For cellular EGFR affinity, A431 epidermoid carcinoma was cultured in DMEM with 10% fetal bovine serum at 37°C in humidified air with 5% CO_2. Cells to be used in flow cytometry were detached using trypsin for a shorter time (3–5 min) than recommended. Detached cells were washed and labeled with $Gp2\text{-}EGFR_{2.2.3}$ at varying concentrations for 15–30 min at 4°C. Cells were pelleted and washed with PBSA (PBS + 0.1% w/v BSA), then labeled with fluorescein-conjugated rabbit anti-His_6 antibody for 15 min at 4°C. For blocking, cells were also labeled with biotin-$Gp2\text{-}EGFR_{2.2.3}$ and detected by Alexa Fluor 647-conjugated streptavidin. Fluorescence was analyzed on a C6 Accuri flow cytometer (BD Biosciences). The equilibrium dissociation constant, K_D, was identified by minimizing the sum of squared errors assuming a 1:1 binding interaction.

SUPPLEMENTAL INFORMATION

Supplemental Information includes Supplemental Experimental Procedures, three figures, and one table and can be found with this article online at http://dx.doi.org/10.1016/j.chembiol.2015.06.012.

ACKNOWLEDGMENTS

We are grateful to Dr. Sivaramesh Wigneshweraraj for the JE1 *E. coli* strain and Aaron Becker at the University of Minnesota Genomics Center for assistance with Illumina sequencing. This work was partially funded by the Department of Defense (Grant W81XWH-13-1-0471 to B.J.H.), the NIH (Grant EB019518 to B.J.H.), and the University of Minnesota.

Received: March 1, 2015
Revised: May 8, 2015
Accepted: June 4, 2015
Published: July 9, 2015

REFERENCES

Ackerman, S.E., Currier, N.V., Bergen, J.M., and Cochran, J.R. (2014). Cystine-knot peptides: emerging tools for cancer imaging and therapy. Expert Rev. Proteomics *11*, 561–572.

Banta, S., Dooley, K., and Shur, O. (2013). Replacing antibodies: engineering new binding proteins. Annu. Rev. Biomed. Eng. *15*, 93–113.

Baum, R.P., Prasad, V., Müller, D., Schuchardt, C., Orlova, A., Wennborg, A., Tolmachev, V., and Feldwisch, J. (2010). Molecular imaging of HER2-expressing malignant tumors in breast cancer patients using synthetic ^{111}In- or ^{68}Ga-labeled affibody molecules. J. Nucl. Med. *51*, 892–897.

Binz, H.K., Amstutz, P., and Plückthun, A. (2005). Engineering novel binding proteins from nonimmunoglobulin domains. Nat. Biotechnol. *23*, 1257–1268.

Bloom, J.D., Labthavikul, S.T., Otey, C.R., and Arnold, F.H. (2006). Protein stability promotes evolvability. Proc. Natl. Acad. Sci. USA *103*, 5869–5874.

Cámara, B., Liu, M., Reynolds, J., Shadrin, A., Liu, B., Kwok, K., Simpson, P., Weinzierl, R., Severinov, K., Cota, E., et al. (2010). T7 phage protein Gp2 inhibits the Escherichia coli RNA polymerase by antagonizing stable DNA strand separation near the transcription start site. Proc. Natl. Acad. Sci. USA *107*, 2247–2252.

Castel, G., Chtéoui, M., Heyd, B., and Tordo, N. (2011). Phage display of combinatorial peptide libraries: application to antiviral research. Molecules *16*, 3499–3518.

Chao, G., Lau, W.L., Hackel, B.J., Sazinsky, S.L., Lippow, S.M., and Wittrup, K.D. (2006). Isolating and engineering human antibodies using yeast surface display. Nat. Protoc. *1*, 755–768.

Chen, J., Sawyer, N., and Regan, L. (2013). Protein-protein interactions: general trends in the relationship between binding affinity and interfacial buried surface area. Protein Sci. *22*, 510–515.

Corcoran, E., and Hanson, R. (2013). Imaging EGFR and HER2 by PET and SPECT: a review. Med. Res. Rev. *2*, 1–48.

Diamond, R. (1974). Real-space refinement of the structure of hen egg-white lysozyme. J. Mol. Biol. *82*, 371–391.

Ederth, J., Artsimovitch, I., Isaksson, L.A., and Landick, R. (2002). The downstream DNA jaw of bacterial RNA polymerase facilitates both transcriptional initiation and pausing. J. Biol. Chem. *277*, 37456–37463.

Engh, R.A., and Bossemeyer, D. (2002). Structural aspects of protein kinase control—role of conformational flexibility. Pharmacol. Ther. *93*, 99–111.

Fleetwood, F., Klint, S., Hanze, M., Gunneriusson, E., Frejd, F.Y., Ståhl, S., and Löfblom, J. (2014). Simultaneous targeting of two ligand-binding sites on VEGFR2 using biparatopic Affibody molecules results in dramatically improved affinity. Sci. Rep. *4*, 7518.

Fraczkiewicz, R., and Braun, W. (1998). Exact and efficient analytical calculation of the accessible surface areas and their gradients for macromolecules. J. Comput. Chem. *19*, 319–333.

Gai, S.A., and Wittrup, K.D. (2007). Yeast surface display for protein engineering and characterization. Curr. Opin. Struct. Biol. *17*, 467–473.

Gebauer, M., and Skerra, A. (2012). Anticalins: small engineered binding proteins based on the lipocalin scaffold. Methods Enzymol. *503*, 157–188.

Gera, N., Hussain, M., Wright, R.C., and Rao, B.M. (2011). Highly stable binding proteins derived from the hyperthermophilic Sso7d scaffold. J. Mol. Biol. *409*, 601–616.

Getz, J.A., Rice, J.J., and Daugherty, P.S. (2011). Protease-resistant peptide ligands from a knottin scaffold library. ACS Chem. Biol. *6*, 837–844.

Grabulovski, D., Kaspar, M., and Neri, D. (2007). A novel, non-immunogenic Fyn SH3-derived binding protein with tumor vascular targeting properties. J. Biol. Chem. *282*, 3196–3204.

Hackel, B.J. (2014). Alternative protein scaffolds for molecular imaging and therapy. In Engineering in Translational Medicine, W. Cai, ed. (Springer), pp. 343–364.

Hackel, B.J., and Wittrup, K.D. (2010). The full amino acid repertoire is superior to serine/tyrosine for selection of high affinity immunoglobulin G binders from the fibronectin scaffold. Protein Eng. Des. Sel. *23*, 211–219.

Hackel, B.J., Kapila, A., and Wittrup, K.D. (2008). Picomolar affinity fibronectin domains engineered utilizing loop length diversity, recursive mutagenesis, and loop shuffling. J. Mol. Biol. *381*, 1238–1252.

Hackel, B.J., Ackerman, M.E., Howland, S.W., and Wittrup, K.D. (2010). Stability and CDR composition biases enrich binder functionality landscapes. J. Mol. Biol. *401*, 84–96.

Hackel, B., Kimura, R., and Gambhir, S. (2012). Use of ^{64}Cu-labeled fibronectin domain with EGFR-overexpressing tumor xenograft: molecular imaging. Radiology *263*, 179–188.

Harris, L.J., Skaletsky, E., and McPherson, A. (1998). Crystallographic structure of an intact IgG1 monoclonal antibody. J. Mol. Biol. *275*, 861–872.

Heinis, C., Rutherford, T., Freund, S., and Winter, G. (2009). Phage-encoded combinatorial chemical libraries based on bicyclic peptides. Nat. Chem. Biol. *5*, 502–507.

Hermeling, S., Crommelin, D.J.A., Schellekens, H., and Jiskoot, W. (2004). Structure-immunogenicity relationships of therapeutic proteins. Pharm. Res. *21*, 897–903.

Hynes, N.E., and MacDonald, G. (2009). ErbB receptors and signaling pathways in cancer. Curr. Opin. Cell Biol. *21*, 177–184.

Koide, A., Bailey, C.W., Huang, X., and Koide, S. (1998). The fibronectin type III domain as a scaffold for novel binding proteins. J. Mol. Biol. *284*, 1141–1151.

Laurent-Puig, P., Cayre, A., Manceau, G., Buc, E., Bachet, J.-B., Lecomte, T., Rougier, P., Lievre, A., Landi, B., Boige, V., et al. (2009). Analysis of PTEN, BRAF, and EGFR status in determining benefit from cetuximab therapy in wild-type KRAS metastatic colon cancer. J. Clin. Oncol. *27*, 5924–5930.

Lipovsek, D. (2011). Adnectins: engineered target-binding protein therapeutics. Protein Eng. Des. Sel. *24*, 3–9.

Lipovsek, D., Lippow, S.M., Hackel, B.J., Gregson, M.W., Cheng, P., Kapila, A., and Wittrup, K.D. (2007). Evolution of an interloop disulfide bond in high-affinity antibody mimics based on fibronectin type III domain and selected by yeast surface display: molecular convergence with single-domain camelid and shark antibodies. J. Mol. Biol. *368*, 1024–1041.

Lobo, E.D., Hansen, R.J., and Balthasar, J.P. (2004). Antibody pharmacokinetics and pharmacodynamics. J. Pharm. Sci. *93*, 2645–2668.

Löfblom, J., Feldwisch, J., Tolmachev, V., Carlsson, J., Ståhl, S., and Frejd, F.Y. (2010). Affibody molecules: engineered proteins for therapeutic, diagnostic and biotechnological applications. FEBS Lett. *584*, 2670–2680.

Malmberg, J., Tolmachev, V., and Orlova, A. (2011). Imaging agents for in vivo molecular profiling of disseminated prostate cancer–targeting EGFR receptors in prostate cancer: comparison of cellular processing of [111In]-labeled affibody molecule Z(EGFR:2377) and cetuximab. Int. J. Oncol. *38*, 1137–1143.

Moore, S.J., Leung, C.L., and Cochran, J.R. (2012). Knottins: disulfide-bonded therapeutic and diagnostic peptides. Drug Discov. Today Technol. *9*, e1–e70.

Moroni, M., Veronese, S., Benvenuti, S., Marrapese, G., Sartore-Bianchi, A., Di Nicolantonio, F., Gambacorta, M., Siena, S., and Bardelli, A. (2005). Gene copy number for epidermal growth factor receptor (EGFR) and clinical response to antiEGFR treatment in colorectal cancer: a cohort study. Lancet Oncol. *6*, 279–286.

Mouratou, B., Schaeffer, F., Guilvout, I., Tello-Manigne, D., Pugsley, A.P., Alzari, P.M., and Pecorari, F. (2007). Remodeling a DNA-binding protein as a specific in vivo inhibitor of bacterial secretin PulD. Proc. Natl. Acad. Sci. USA *104*, 17983–17988.

Natarajan, A., Hackel, B.J., and Gambhir, S.S. (2013). A novel engineered anti-CD20 tracer enables early time PET imaging in a humanized transgenic mouse model of B-cell non-Hodgkins lymphoma. Clin. Cancer Res. *19*, 6820–6829.

Nechaev, S., and Severinov, K. (1999). Inhibition of *Escherichia coli* RNA polymerase by bacteriophage T7 gene 2 protein. J. Mol. Biol. *289*, 815–826.

Orlova, A., Wållberg, H., Stone-Elander, S., and Tolmachev, V. (2009). On the selection of a tracer for PET imaging of HER2-expressing tumors: direct comparison of a ^{124}I-labeled affibody molecule and trastuzumab in a murine xenograft model. J. Nucl. Med. *50*, 417–425.

Panni, S., Dente, L., and Cesareni, G. (2002). In vitro evolution of recognition specificity mediated by SH3 domains reveals target recognition rules. J. Biol. Chem. *277*, 21666–21674.

Pavoor, T.V., Cho, Y.K., and Shusta, E.V. (2009). Development of GFP-based biosensors possessing the binding properties of antibodies. Proc. Natl. Acad. Sci. USA *106*, 11895–11900.

Reilly, R.M., Kiarash, R., Sandhu, J., Lee, Y.W., Cameron, R.G., Hendler, A., Vallis, K., and Gariépy, J. (2000). A comparison of EGF and MAb 528 labeled with ^{111}In for imaging human breast cancer. J. Nucl. Med. *41*, 903–911.

Revets, H., De Baetselier, P., and Muyldermans, S. (2005). Nanobodies as novel agents for cancer therapy. Expert Opin. Biol. Ther. *5*, 111–124.

Roldan, J.L.O., Blackledge, M., van Nuland, N.A.J., and Azuaga, A.I. (2011). Solution structure, dynamics and thermodynamics of the three SH3 domains of CD2AP. J. Biomol. NMR *50*, 103–117.

Rosenberg, A.S. (2006). Effects of protein aggregates: an immunologic perspective. AAPS J. *8*, E501–E507.

Scartozzi, M., Bearzi, I., Mandolesi, A., Pierantoni, C., Loupakis, F., Zaniboni, A., Negri, F., Quadri, A., Zorzi, F., Galizia, E., et al. (2009). Epidermal Growth Factor Receptor (EGFR) gene copy number (GCN) correlates with clinical activity of irinotecan-cetuximab in K-RAS wild-type colorectal cancer: a fluorescence in situ (FISH) and chromogenic in situ hybridization (CISH) analysis. BMC Cancer *9*, 303.

Schmidt, M.M., and Wittrup, K.D. (2009). A modeling analysis of the effects of molecular size and binding affinity on tumor targeting. Mol. Cancer Ther. *8*, 2861–2871.

Sidhu, S.S. (2012). Antibodies for all: the case for genome-wide affinity reagents. FEBS Lett. *586*, 2778–2779.

Spangler, J.B., Neil, J.R., Abramovitch, S., Yarden, Y., White, F.M., Lauffenburger, D.A., and Wittrup, K.D. (2010). Combination antibody treatment down-regulates epidermal growth factor receptor by inhibiting endosomal recycling. Proc. Natl. Acad. Sci. USA *107*, 13252–13257.

Stern, L., Case, B., and Hackel, B. (2013). Alternative non-antibody protein scaffolds for molecular imaging of cancer. Curr. Opin. Chem. Eng. *2*, 425–432.

Tamaskovic, R., Simon, M., Stefan, N., Schwill, M., and Plückthun, A. (2012). Designed ankyrin repeat proteins (DARPins) from research to therapy. Methods Enzymol. *503*, 101–134.

Thurber, G., Schmidt, M., and Wittrup, K. (2008a). Antibody tumor penetration: transport opposed by systemic and antigen-mediated clearance. Adv. Drug Deliv. Rev. *60*, 1421.

Thurber, G.M., Schmidt, M.M., and Wittrup, K.D. (2008b). Factors determining antibody distribution in tumors. Trends Pharmacol. Sci. *29*, 57–61.

Wu, A.M., and Senter, P.D. (2005). Arming antibodies: prospects and challenges for immunoconjugates. Nat. Biotechnol. *23*, 1137–1146.

Yin, S., Ding, F., and Dokholyan, N. (2007). Eris: an automated estimator of protein stability. Nat. Methods *4*, 466–467.

Yuan, F., Dellian, M., Fukumura, D., and Leunig, M. (1995). Vascular permeability in a human tumor xenograft: molecular size dependence and cutoff size. Cancer Res. *55*, 3752–3756.

Zahnd, C., Kawe, M., Stumpp, M.T., de Pasquale, C., Tamaskovic, R., Nagy-Davidescu, G., Dreier, B., Schibli, R., Binz, H.K., Waibel, R., et al. (2010). Efficient tumor targeting with high-affinity designed ankyrin repeat proteins: effects of affinity and molecular size. Cancer Res. *70*, 1595–1605.

Zhang, Y., and Skolnick, J. (2005). TM-align: a protein structure alignment algorithm based on the TM-score. Nucleic Acids Res. *33*, 2302–2309.

